Pol. J. Environ. Stud. Vol. 26, No. 2 (2017), 871-880
DOI: *10.15244/pjoes/65363*

Original Research

Hierarchical Ag-ZnO Microspheres with Enhanced Photocatalytic Degradation Activities

Hua-Yi Wu[1], Wen-Jie Jian[1], Hai-Feng Dang[2], Xiu-Feng Zhao[3], Li-Zhong Zhang[3], Jian-Hui Li[3, 4]*

[1]Department of pharmacy, Xiamen Medical College, Xiamen 361008, China
[2]College of Chemistry and Environmental Engineering, Guangdong Engineering and Technology Research Center for Advanced Nanomaterials, Dongguan University of Technology, Dongguan 523808, China
[3]Department of Chemistry and Applied Chemistry, Changji University, Changji 831100, China
[4]State Key Laboratory of Physical Chemistry of Solid Surfaces, National Engineering Laboratory for Green Chemical Productions of Alcohols, Ethers and Esters, and Department of Chemistry, College of Chemistry and Chemical Engineering, Xiamen University, Xiamen 361005, China

Received: 26 July 2016
Accepted: 26 September 2016

Abstract

In this work, the significantly enhanced photocatalytic performances and higher reaction rate of the hierarchical ZnO microspheres – initially prepared by a solvothermal method without surfactants or templates and decorated with Ag nanoparticles by a photoreduction method – were found for the degradation of methylene blue (MB) under both ultraviolet (UV) and visible light irradiation. Various characterization results confirmed that the modification of silver with an optimal amount can effectively extend the absorption spectrum to the visible region and inhibit a recombination of photo-induced charge carriers. Moreover, the reason for promoted photostability and the possible mechanism for the enhanced photocatalytic activity of the as-prepared Ag/ZnO composites under UV or visible light irradiation were also systematically investigated and discussed.

Keywords: hierarchical, photodegradation, visible light, Ag/ZnO composites, microspheres

Introduction

Recently, as a potential solution handling environmental pollutants, photo-catalysis using an effective semiconductor has been a research focus, particularly for the elimination of hazardous materials in polluted water [1-2]. Among various semiconductors, ZnO has been considered as an excellent photocatalyst candidate with respect to its high photosensitivity, non-toxicity, abundant availability, low cost, etc. [3-4]. However, the practical application of unitary ZnO materials still confronts two challenges, i.e., the limited absorption spectrum range within UV light (λ<387 nm) [5] and severe recombination of

*e-mail: jhli@xmu.edu.cn

photogenerated electron-hole pairs resulting in relatively low quantum yields [6].

So far, diverse strategies have been explored to overcome the aforementioned drawbacks, including surface alteration [7], formation of heterostructures [8-10] or nanocomposites [11-12] modified with polymer [13] or metals [14-15], etc. Many researchers have demonstrated a significantly extended light-absorption range and prolonging the lifetimes of photoexcited charge carriers through the decoration of noble metal nanoparticles onto ZnO [16-19]. This is mainly due to the respective effects of surface plasmon resonance (SPR) and the formation of a Schottky barrier at the metal-ZnO interface. Among the noble metals investigated, nano Ag plays a crucial role in the enhancement of photocatalytic performance for the degradation of organic dyes [17, 20].

The nanostructured semiconductor has attracted increasing attention as one of the promising photocatalysts for its large surface area and large number of active sites. However, nanosized materials with high surface-to-volume ratios suffer significantly from aggregation, deactivation, and recyclability in aqueous photocatalytic reactions. Compared with powder-like nanoparticles, photocatalysts with hierarchical microsphere structure could present superior performance in the photocatalytic reaction because of their low density, high surface area, easy settlement, good delivering ability, and surface permeability [21-25].

Ag-ZnO composites are usually synthesized using the "one-pot" method by co-heat-treatment of mixed Ag and Zn precursor at high temperature [26-27] which, however, suffers from the restrictions of the time-consuming process and uncontrolled Ag particle sizes. It has been reported that the silver ion can be reduced to metallic Ag and deposited onto the substrate surface by the photogenerated electron in the solution – the so-called photoreduction method [28-29], which is proved to be simple, efficient, and low-cost. Furthermore, as mentioned above, the assembled hierarchical microsphere structures for modified ZnO have an overall dimension in micrometers and are stable enough to resist agglomeration. The photocatalytic activities of the assembled structures will be maintained for the existence of nanosized catalytic active units or even higher, since more lights scattered over the hierarchical microsphere structure will lead to better light adsorption. Therefore, decorated Ag nanoparticles on the surface of ZnO microspheres forming a hierarchical photocatalyst using the simple photoreduction method is an important and interesting area of research.

Herein, the catalytic active Ag-modified ZnO hierarchical microspheres with enhanced stability were successfully synthesized. The ZnO substrate self-assembled of ZnO nanoparticles was prepared via a facile and template-free approach. The Ag particles were decorated onto the ZnO surfaces by photoreduction of Ag ions. The photocatalytic activity and stability were tested with and applied to the degradation of methylene blue (MB) as a probe reaction. The possible mechanism for the desirable photocatalytic activity of Ag/ZnO composites under UV or visible light irradiation was also proposed.

Materials and Method

Synthesis of Hierarchical ZnO Microspheres

Typically, 0.48 mmol zinc nitrate hexahydrate ($Zn(NO_3)_2 \cdot 6H_2O$), 0.26 mmol methenamine ($(CH_2)_6N_4$), and 0.06 mmol trisodium citrate ($C_6H_5Na_3O_7 \cdot 2H_2O$) were dissolved in 50 mL distilled water. After being sonicated for 5 min, the mixture was then heated at 90°C for 2 h and then aged at ambient temperature for 10 h. The resulting precipitates were obtained by centrifugation, washed with ethanol and deionized water, and then dried at 60ºC for 10 h. Subsequently, the final hierarchical ZnO microspheres were achieved through a heat treatment of the precursors at 450ºC in air for 30 min.

Synthesis of Ag-Modified ZnO Microspheres

For the preparation of Ag-modified ZnO microspheres (denoted as Ag/ZnO), 0.2 g of the synthesized ZnO microspheres was dispersed into 100 mL distilled water by sonication for 20 min, followed by the addition of different amounts of $AgNO_3$. The above suspension was stirred in the dark for 0.5 h and then irradiated for 0.5 h by employing a high-pressure Hg UV lamp. Then the mixture was centrifuged and washed with distilled water and alcohol several times. The products were dried at 60ºC for 12 h. The precise Ag contents of the Ag/ZnO composites were determined by the AAS analysis and the results are listed in Table 1. Therefore, the Ag/ZnO composites prepared with different $AgNO_3$ concentrations of 0.3 mmol, 0.6 mmol, 1.2 mmol, and 2.4 mmol are hereafter denoted as 5.41 wt% Ag/ZnO, 7.95 wt% Ag/ZnO, 10.03 wt% Ag/ZnO, and 11.37 wt% Ag/ZnO, respectively.

Characterization

X-ray diffraction (XRD) measurement was carried out by a RigakuUltima IV x-ray diffractometer with Cu-Ka radiation ($\lambda = 0.15418$ nm) for phase identification. The morphologies of the products were investigated by a Hitachi S-4800 field-emission scanning electron microscope (SEM) and TECNAI F-30 FEG transmission

Table 1. The Ag contents in various Ag/ZnO samples.

Sample	$AgNO_3$ / mmol	Irradiation time / min	Ag / wt%
1	0.3	30	5.41
2	0.6	30	7.95
3	1.2	30	10.03
4	2.4	30	11.37

electron microscope (TEM). Chemical compositions were measured by x-ray energy-dispersive spectroscopy (EDS) equipped with TEM. The silver contents in the Ag/ZnO composites were quantified by a Shimadzu Model AA-670 flame atomic absorption spectrometer. N_2 adsorption/desorption isotherms were recorded at 77 K on an automated micromeritics Tri-Star 3000 apparatus. Surface areas were calculated using the multipoint BET equation. Fourier transforms infrared spectrometer (FT-IR) spectra were recorded in KBr dispersion in the range of 400 to 4,000 cm^{-1}. The surface compositions of the samples were obtained from x-ray photoelectron spectroscopy (XPS) using a VG ESCALAB/Auger. UV/vis absorption spectra were recorded with a UV-vis spectrophotometer (Cary 5000) with an integrating sphere attachment and $BaSO_4$ as a reflectance standard. The photoluminescence (PL) spectra were measured on a Hitachi F-7000 luminescence spectrometer at room temperature.

Photocatalytic Activities Test

The photocatalytic performance of the ZnO and Ag/ZnO samples were evaluated by examining the degradation of methylene blue (MB) chosen as model chemical. A high-pressure Hg UV lamp (250 W) with a maximum emission at 365 nm served as the UV resource for UV light photocatalysis. A 500 W Xenon lamp with a filter (420 nm) to cut off the UV light was used as the visible light source. Typically, 20 mg of the catalysts (Ag/ZnO or ZnO) were ultrasonically dispersed into 40 mL aqueous suspensions of MB (10 mg/L). Prior to irradiation, the mixture was stirred in the dark for 30 min to establish an adsorption/desorption equilibrium. After a given irradiation time, a certain amount of solutions was collected and centrifuged to remove the photocatalysts. Subsequently, the residual MB concentration was tested by a UV-vis spectrophotometer.

Results and Discussion

XRD patterns of ZnO and Ag/ZnO microspheres with different Ag content are shown in Fig. 1. All the diffraction peaks in Fig. 1a) can be perfectly assigned to wurtzite-structured ZnO (JCPDS NO. 36-1451). As shown in Figs. 1b-e), two sets of diffraction peaks existed for all the Ag-modified samples, which were attributed to the wurtzite-structured ZnO and face-centered cubic sliver (JCPDS NO. 04-0783) [30-32]. The diffraction peaks of Ag were strengthened gradually when the Ag content in the composites increased from 5.41 to 11.37 wt%. No additional peaks for impurity were detected, suggesting that the Ag/ZnO composites were composed of Ag and ZnO.

Fig. 2 shows the SEM and TEM images of as-prepared ZnO and Ag/ZnO composites. As shown in Fig. 2a), the ZnO samples mainly consist of hierarchical microspheres with an average size of approximately 2 μm. The highly magnified SEM image of a fragment of the sphere

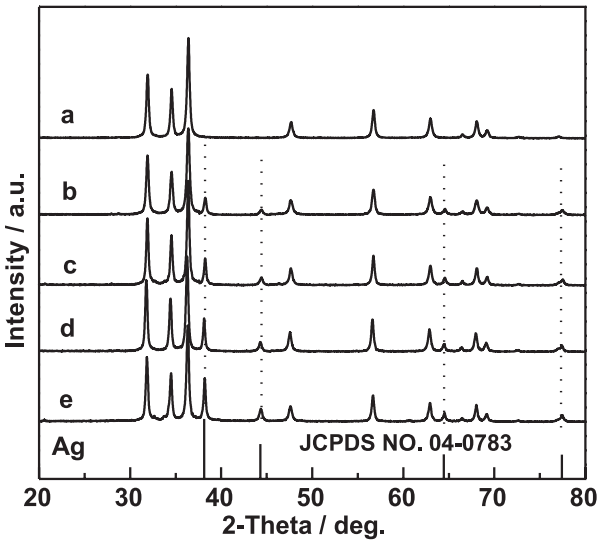

Fig. 1. The XRD patterns of a) ZnO, b) 5.41 wt% Ag/ZnO, c) 7.95 wt% Ag/ZnO, d) 10.03 wt% Ag/ZnO, and e) 11.37 wt% Ag/ZnO.

(Fig. 2b) exhibits that the architecture of the hierarchical ZnO microsphere are built from numerous oriented nanoparticles. A large number of pores are engendered in the microspheres, which can increase the accessible surface area of the materials and is conducive to the transport of small molecules. Figs 2 (c, d) exhibit the SEM images of

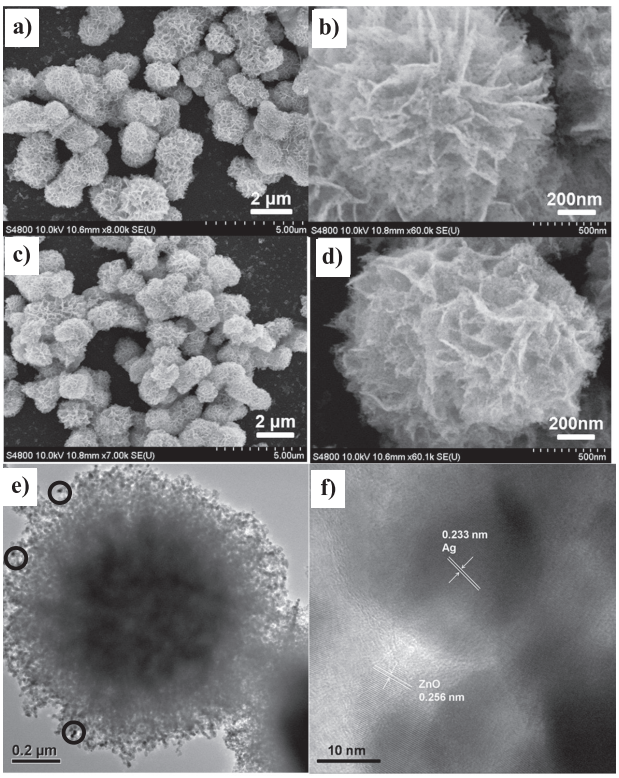

Fig. 2. The SEM images of (a, b) hierarchical ZnO microspheres, (c, d) 10.03 wt% Ag/ZnO, e) TEM, and f) HRTEM images of 10.03 wt% Ag/ZnO samples.

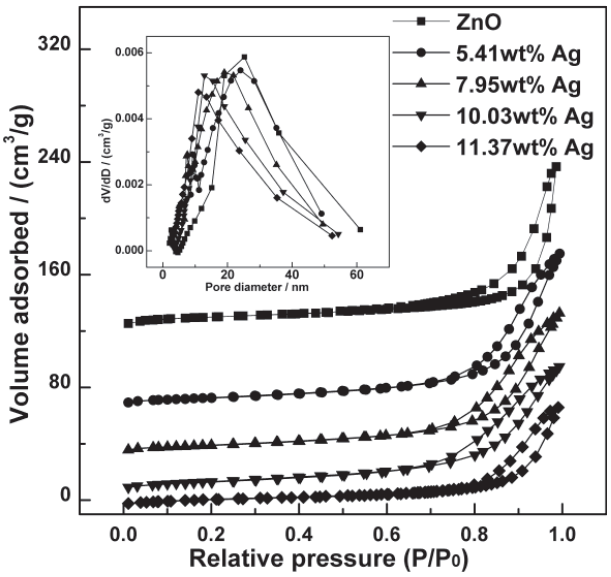

Fig. 3. N_2 adsorption-desorption isotherm and BJH pore diameter distribution (inset) of ZnO- and Ag-doped ZnO.

Ag/ZnO composites. It is clear that the morphology of ZnO remains unchanged after Ag modification. The TEM image, as shown in Fig. 2e), further confirms the results obtained from SEM observations. The original structure is well inherited by the Ag/ZnO microspheres, and numerous nanopores can also be observed. In addition, many spherical Ag nanoparticles appear on the surface of the ZnO microsphere. To achieve more convincible evidence, the HRTEM image of the Ag/ZnO sample is depicted in Fig. 2f). The interplanar spacing of about 0.256 nm can be assigned to the (002) plane of ZnO, while the interplanar spacing of 0.233 nm corresponds to the (111) plane of Ag. Energy-dispersive X-ray spectroscopy (EDS) analysis also confirms that the Ag/ZnO composites only contain silver, zinc, and oxygen elements, which is consistent with the above-mentioned conclusion.

The nitrogen desorption/adsorption isotherms of the samples are shown in Fig. 3. The isotherms correspond to the type IV with H3-type hysteresis loop, indicating the existence of mesopores (2-50 nm). The inset in Fig. 3 exhibits the pore diameter distribution. It is clear that all the samples present in mesopores have diameters in the range of 2-50 nm. All the BET surface areas of ZnO and Ag-modified ZnO are around 30 $m^2 \cdot g^{-1}$, and the presence of Ag NPs does not obviously impact the BET surface area of the photocatalysts.

The chemical component of the as-obtained 10.03 wt% Ag/ZnO sample was investigated by X-ray photoelectron spectroscopy (XPS) analysis and the corresponding results are shown in Fig. 4. It is clear that all of the peaks on the curve can be assigned to Zn, O, Ag, and C elements and no peaks of other elements can be observed (Fig. 4a). The existence of the C element could be ascribed to the hydrocarbon contaminants. The high-resolution Zn 2p spectrum is analyzed in Fig. 4b. The binding

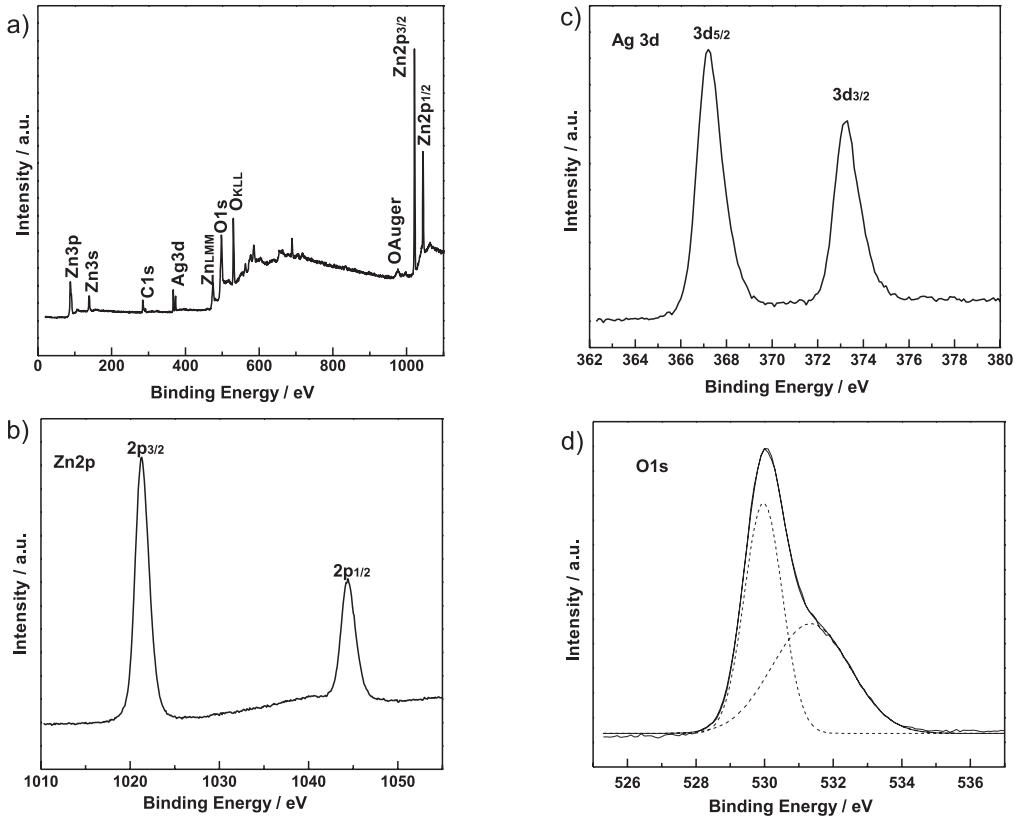

Fig. 4. Complete XPS spectra of a) 10.03 wt% Ag/ZnO sample and high-resolution spectra of sample for the elements of b) Zn, c) Ag, and d) O.

energies of Zn $2p_{3/2}$ and Zn $2p_{1/2}$ are located at 1021.3 and 1044.4 eV, which indicates that the Zn element is mainly in the form of Zn^{2+} on the surface [33]. Fig. 4c displays the high-resolution Ag 3d spectrum. The peak at 367.2 eV is assigned to Ag $3d_{5/2}$ and the peak at 373.2 eV corresponds to Ag $3d_{3/2}$. And the binding energies of Ag $3d_{5/2}$ and $3d_{3/2}$ peaks for the composites all shift to lower values compared with those of bulk silver (Ag $3d_{5/2}$, 368.2 eV; Ag $3d_{3/2}$, 374.2 eV [34,35]). The similar phenomenon is also obtained from worm-like Ag/ZnO heterostructural composites and Ag-ZnO heterostructural nanoparticles [20, 36]. Such a shift is primarily due to the strong interaction between Ag and ZnO. The functional work of Ag metallic (4.26 eV) is lower than that of ZnO (5.3 eV), which will steer electrons from Ag to ZnO at the interfaces of Ag-ZnO composites, leading to the higher valance of Ag when Ag nanoparticles are attached to ZnO microspheres. Obviously, the O1s peak exhibited in Fig. 4d is asymmetric and thus it can be deconvoluted into two symmetrical peaks. The binding energy at 531.4 eV is associated with chemisorbed oxygen of the surface hydroxyls and the 530.1 eV peak is associated with the lattice oxygen of ZnO [37].

Fig. 5 shows the UV-vis reflectance spectra of hierarchical ZnO microspheres and the Ag/ZnO composites with various Ag contents. In the range of 200-800 nm, two absorption bands can be observed for the Ag/ZnO composites. The absorption band located at the UV region can be ascribed to the absorption of ZnO and the absorption peak fell in visible range is thought to be the characteristic absorption of surface plasmon resonance (SPR) caused by silver nanoparticles [38-39]. The SPR effect tends to strengthen with the increasing of Ag content and can enhance the visible light absorption ability of the catalysts. Furthermore, it also means the possibility of the Ag/ZnO composites used as a visible light-driven photocatalyst.

The PL spectrum is an effective method to characterize the optical and photochemical properties of semiconductor materials. It can offer important information corresponding to the separation and recombination of photoinduced charge carriers of photocatalysts. Fig. 6 exhibits the room-temperature PL spectra of the as-prepared ZnO and the Ag/ZnO composites with different Ag contents. It is clear that the PL intensity of Ag/ZnO composites decreases sharply in emission yield compared to pure ZnO – both in the UV and visible light regions. This means that the PL quenching effect occurs when Ag particles are introduced to the ZnO microspheres. The quenching effect of the Ag/ZnO composites is arranged in the following order: 10.03 wt% Ag/ZnO > 11.37 wt% Ag/ZnO >7.95wt% Ag/ZnO > 5.41wt% Ag/ZnO. This result could be rationalized by the fact that Ag on the surface of ZnO may act as electron trappers to separate the electron-hole pairs at low loading. With increasing Ag content (from 5.41 to 10.03 wt%), more metal sites favored to trap the electrons are formed and this leads to the enhancement in separation effects for the photoinduced electrons and holes, and thus a decrease intensity of PL emission. When the Ag content exceeds a certain amount (>10.03 wt%), an abnormal change occurs. This can be ascribed to the absorption or reflection of emission at the Ag/ZnO interface, which is induced by the strong surface plasmon absorption of Ag particles [27, 40]. Among all the samples, 10.03wt% Ag/ZnO shows the lowest intensity of PL, indicating the highest separation efficiency of photogenerated electron-hole pairs. The photocatalytic activity of the Ag/ZnO composites will be improved if the separation efficiency of photogenerated electron-hole pairs in the Ag/ZnO composites is higher.

Catalytic Performance

The photocatalytic performances of the hierarchical ZnO microspheres and Ag/ZnO were evaluated by photodegrading MB solution, which is a typical organic pollutant from the textile industry. Under UV irradiation, the photocatalytic results of MB in the presence of different

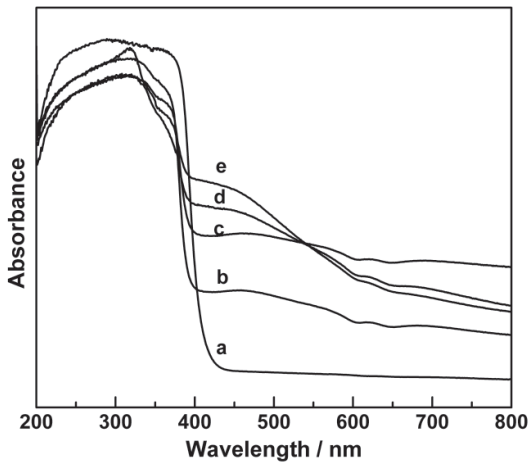

Fig. 5. UV-vis absorption spectra of a) ZnO, b) 5.41wt% Ag/ZnO, c) 7.95wt% Ag/ZnO, d) 10.03wt% Ag/ZnO, and e) 11.37wt% Ag/ZnO.

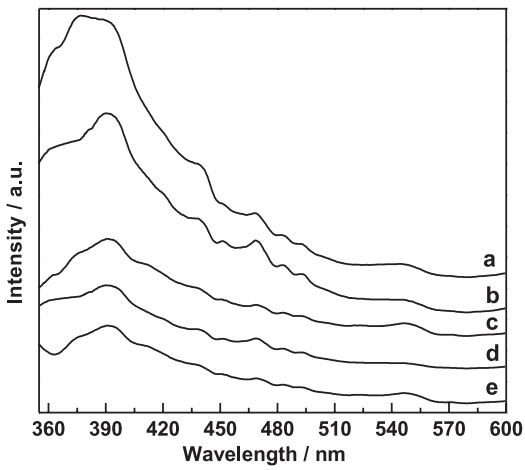

Fig. 6. PL spectra of a) ZnO, b) 5.41wt% Ag/ZnO, c) 7.95wt% Ag/ZnO, d) 10.03wt% Ag/ZnO, and e) 11.37wt% Ag/ZnO.

catalysts (as-prepared ZnO and Ag/ZnO composites) are all exhibited in Fig. 7a. In the absence of the catalyst, the degradation rate of MB under UV irradiation is extremely slow and thus photolysis can be ignored. Pure ZnO microspheres only display a moderate activity. However, the addition of Ag effectively enhances the photocatalytic performance. After exposure to UV light for 20 min, the degradation efficiencies of MB are as follows: 78.8% for pure ZnO, 90.2% for 5.41wt% Ag/ZnO, 94.2% for 7.95wt% Ag/ZnO, 99.2% for 10.03 wt% Ag/ZnO, and 96.0% for 11.37wt% Ag/ZnO. It is obvious that all Ag/ZnO composites show superior activity over pure ZnO and the activity of Ag/ZnO samples firstly increase and then decrease with the increase of Ag content in the composites. The 10.03 wt% Ag/ZnO composite possesses the best performance, which is in accordance with the PL results.

The photodegradation of MB can be described as a pseudo-first-order reaction [41], for which the kinetic reaction can be expressed as $\ln (C_0/C) = kt$, where C_0 is the initial MB concentration, C is the residual MB concentration at different illumination intervals, k is the pseudo-first-rate kinetic constant (min^{-1}), and t represents the irradiation time. The kinetic constant k under UV irradiation conditions and the square of correlation coefficient of kinetic linear fitting are listed in Table 2. From the results, it is clear that k value for all the Ag/ZnO composites is higher than that for pure ZnO microspheres. The 10.03 wt% Ag/ZnO sample achieves the optimal photocatalytic performance and the k value of 10.03 wt% Ag/ZnO sample is two times higher than that of pure ZnO microspheres. These results confirm that the catalytic performance of ZnO is enhanced by the modification of Ag-NPs.

Fig. 7 (c, d) exhibit the catalytic performance and the kinetics of the pure ZnO microspheres and Ag/ZnO composites for degradation of MB under visible light irradiation. The obtained k values and the square values of correlation coefficient for various catalysts are present in Table 2. In the entire irradiation process, less than 3% of MB is degraded without any photocatalysts. The 10.03 wt% Ag/ZnO sample shows the most superior activity, of which k value is much higher than that of pure ZnO microspheres. With the increase of Ag content (from 5.41 to 10.03 wt%), the photocatalytic performance and k value have also been increased. Nevertheless, the catalytic efficiency and k value decline when Ag content is further increased (11.37 wt%). This result is similar

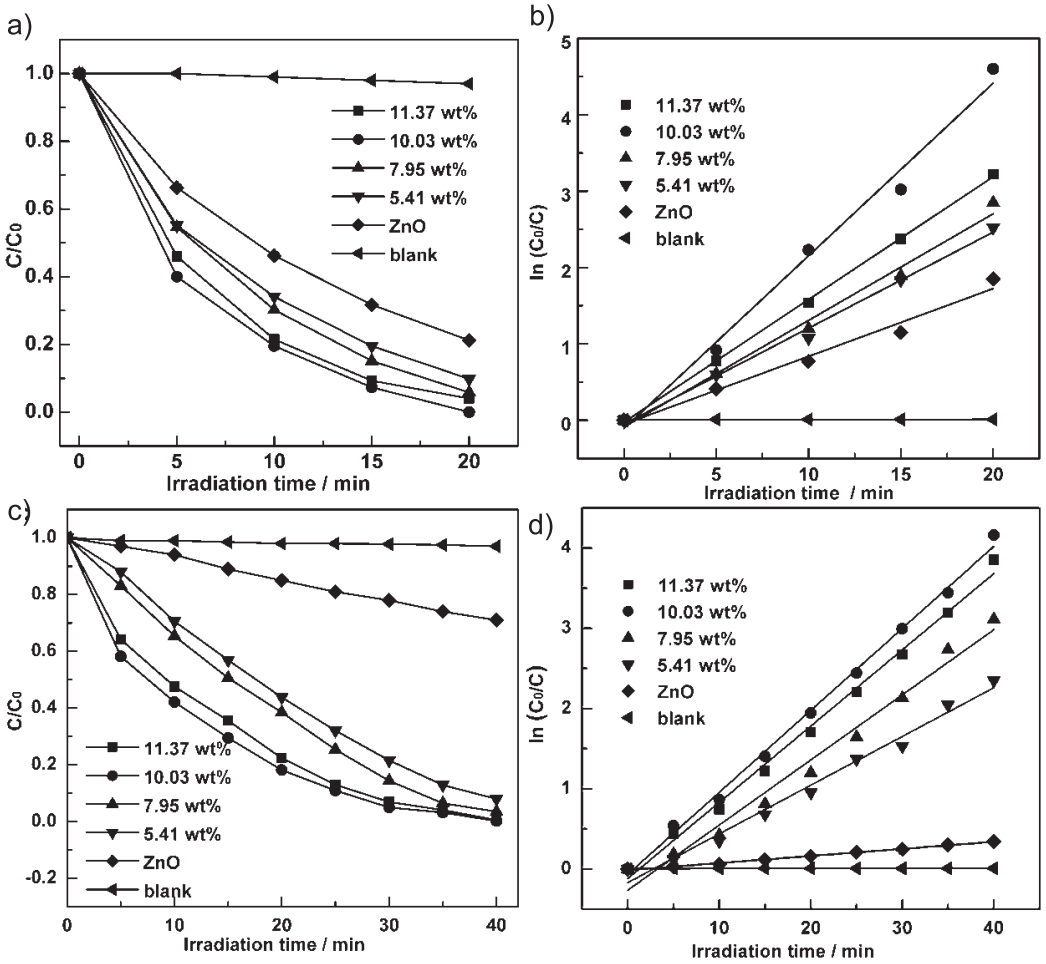

Fig. 7. a), c) Photocatalytic activity and b), d) kinetics of the obtained ZnO microspheres and Ag/ZnO composites prepared with various Ag contents for degradation of MB under a), b) UV, and c), d) visible light.

Table 2. Reaction rate constant (k) for photocatalytic degradation of MB under UV and visible light irradiation.

Irradiation	Constant	ZnO	5.41wt% Ag/ZnO	7.95wt% Ag/ZnO	10.03wt% Ag/ZnO	11.37wt% Ag/ZnO
UV light	k / min^{-1}	0.0888	0.1257	0.1396	0.2261	0.1607
	$R^{2\,a}$	0.9899	0.9921	0.9854	0.9563	0.9992
Visible light	k / min^{-1}	0.0088	0.0607	0.0830	0.1022	0.0950
	$R^{2\,a}$	0.9904	0.9836	0.9886	0.9961	0.9934

[a] R^2: the square of correlation coefficient of kinetic linear fitting.

to the activity investigated under UV irradiation. When Ag is incorporated into ZnO, two different phenomena would occur. For Ag content ≤ 10.03 wt%, Ag particles loaded on ZnO might act as an electron accepter and the electrons on the surface of ZnO could effectively transfer to Ag particles. In contrast, at higher Ag content, some Ag particles might reversibly act as the recombination centers of electrons and holes and thus reduce the photocatalytic efficiency of the catalyst. Similar results are also observed in the literature [20, 40].

For the purpose of the application, it is crucial for the photocatalyst to maintain superior photocatalytic activity and stability over a long period of time. As Fig. 8 illustrates, the 10.03 wt% Ag/ZnO sample exhibits effective photocatalytic performance under UV and visible light irradiation. There is insignificant loss of the photocatalytic efficiency after four cycles, indicating the highly stable and reusable of the 10.03 wt% Ag/ZnO sample. The SEM images of the used 10.03 wt% Ag/ZnO sample present that this sample still maintains the original structure even after several recycles. The possible reason for the favorable photocatalyst is that the hierarchical microspheres have an overall dimension in micrometers with nanosized units that are stabilized to ensure superior structural stability [36, 42].

Photocatalytic Mechanism

On the basis of the aforementioned results and the theory analysis [16], a proposed mechanism diagram

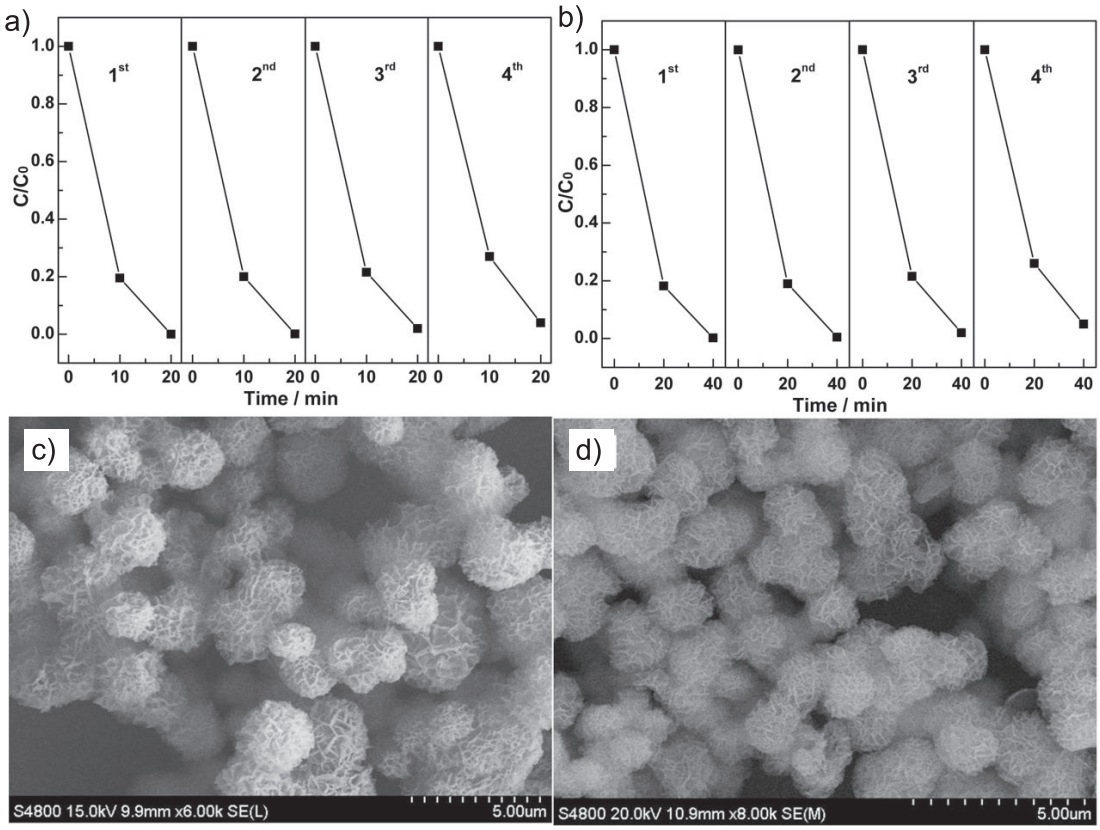

Fig. 8. Recycle degradation of MB performance of 10.03 wt% Ag/ZnO sample under a) UV and b) visible light irradiation and the SEM images of the 10.03 wt% Ag/ZnO sample that had been reused after four cycles under c) UV and d) visible light irradiation.

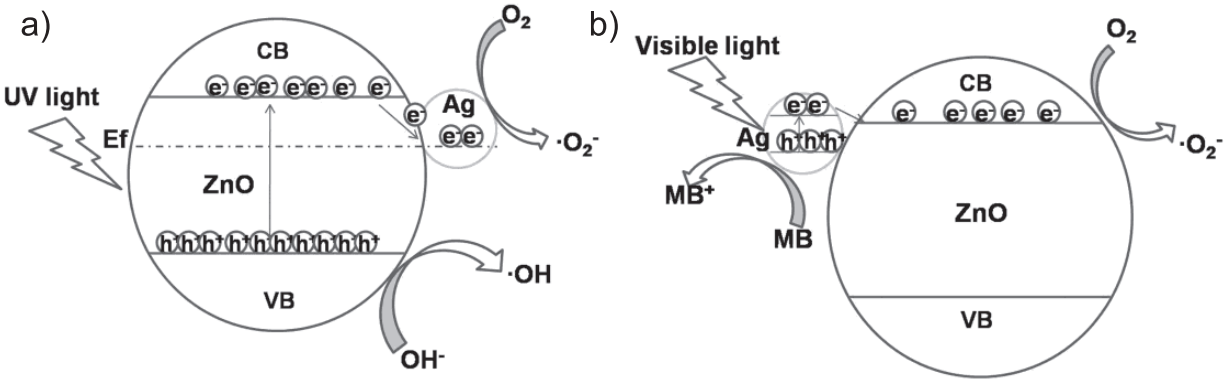

Fig. 9. Schematic diagram of photocatalytic mechanism Ag/ZnO composites under UV a) and visible light b) irradiation.

of the enhanced photocatalytic performance of the Ag/ZnO composites under UV and visible light irradiation is illustrated schematically in Fig. 9.

The improved photocatalytic efficiency of the Ag/ZnO heterostructure under UV irradiation can be mainly ascribed to the formation of the Schottky barriers at metal-semiconductor interface between Ag particles and hierarchical ZnO microspheres, which are propitious to the segregation of charges and inhibited the charge recombination. When Ag/ZnO composites are illuminated by UV light with photo energy equal to or higher than the band gap of ZnO, the ZnO microspheres could be simultaneously excited to form electron-hole pairs. As shown in Fig. 9a, the photogenerated electron in the CB of ZnO could migrate to Ag particles due to the driving force produced by the deflexed energy band in the space charge region. Ag particles, acting as electron sinks, not only reduce the recombination ratio of electron-hole pairs but also increase the lifetime of the photogenerated pairs. Then the absorbed O_2 and H_2O on the surface of the Ag/ZnO composites would react with the photogenerated electrons to form superoxide radical anions such as $\cdot O_2$-, $\cdot HO_2$, and $\cdot OH$. The photoinduced holes are inclined to interact with OH^- or H_2O to further generate $\cdot OH$ species, which has a strong oxidizability to decompose most of the pollutants [43-44].

The photocatalytic process under visible light irradiation for the Ag/ZnO composites can be interpreted by the proposed mechanism shown in Fig. 9b. When the Ag/ZnO composites are exposed to visible light, Ag particles would capture the photons due to the strong SPR effect, which results in the formation of electron-hole pairs in the Ag particles. Subsequently, the photoinduced electrons transfer from Ag to the CB of ZnO and then these injected electrons are consumed by the O_2 dissolved in the solution to yield various reactive oxidative species [16, 45]. Photodegradation of MB could subsequently take place through the attack of reactive oxidative species.

On the basis of the above-mentioned results, it is obvious that the optimal Ag content for preparing Ag/ZnO composites with a superior catalytic performance is about 10.03 wt%, which can effectively hinder the recombination of photoinduced electron-hole pairs to achieve the best photocatalytic performance. Besides, from Figs 6 and 7 it is clear that the order of PL intensities of the samples is just opposite that of the photocatalytic performance, confirming the occurrence of the separation effect between the photogenerated electrons and holes.

Conclusions

Hierarchical Ag/ZnO microspheres with different Ag content were successfully synthesized via a facile two-step method. The as-prepared Ag/ZnO composites exhibited superior photocatalytic activity over pure ZnO microspheres on the degradation of MB under UV or visible light irradiation. After being used four times, more than 90% of degradation efficiency could also be maintained. The characterization results showed that the enhanced photocatalytic performance and high photostability could be ascribed to the incorporation of Ag nanoparticles and the unique hierarchical structure. The Ag nanoparticles located on the surface of the ZnO microspheres acted as electron sinks to improve the charge separation and extend the light-absorption range through surface plasmon resonance effect.

Acknowledgements

This work was supported by the National Basic Research Program of China (2013CB933102) and Natural Science Project of Xiamen Medical College (K2016-15).

References

1. XU F., YUAN Y., HAN H., WU D., GAO Z., JIANG K. Synthesis of ZnO/CdS hierarchical heterostructure with enhanced photocatalytic efficiency under nature sunlight. Crystengcomm, **14**, 3615, **2012**.
2. HAN Z., REN L., CUI Z., CHEN C., PAN H., CHEN J. Ag/ZnO flower heterostructures as a visible-light driven photocatalyst via surface plasmon resonance. Applied Catalysis B: Environmental. **126**, 298, **2012**.

3. ZHANG H., CHEN G., BAHNEMANN D.W. Photoelectrocatalytic materials for environmental applications, Journal of Materials Chemistry. **19**, 5089, **2009**.
4. KAYACI F., VEMPATI S., DONMEZ I., BIYIKLI N., UYAR T. Role of zinc interstitials and oxygen vacancies of ZnO in photocatalysis: a bottom-up approach to control defect density. Nanoscale, **6**, 10224, **2014**.
5. BEGUM G., MANNA J., RANA R.K. Controlled Orientation in a Bio-Inspired Assembly of Ag/AgCl/ZnO Nanostructures Enables Enhancement in Visible-Light-Induced Photocatalytic Performance. Chemistry-A European Journal, **18**, 6847, **2012**.
6. LIU Y., WEI S., WEI G. Ag/ZnO heterostructures and their photocatalytic activity under visible light: Effect of reducing medium. Journal of Hazardous Materials, **287**, 59, **2015**.
7. LI Y., ZHOU X., HU X., ZHAO X., FANG P. Formation of Surface Complex Leading to Efficient Visible Photocatalytic Activity and Improvement of Photostabilty of ZnO. Journal of Physical Chemistry C, **113**, 16188, **2009**.
8. JIN J.J., YU J.G., GUO D.P., CUI C., HO W.K. A Hierarchical Z-Scheme CdS-WO_3 photocatalyst with Enhanced CO_2 reduction Activity. Small, **11**, 5262, **2015**.
9. LI J.D., YU C.L., FANG W., ZHU L.H., ZHOU W.Q., FAN Q.Z., Preparation, characterization and photocatalytic performance of heterostructured AgCl/Bi_2WO_6 microspheres. Chinese Journal of Catalysis, **36**, 987, **2015**.
10. KAYACI F., VEMPATI S., OZGIT-AKGUN C., DONMEZ I., BIYIKLI N., UYAR T. Selective isolation of the electron or hole in photocatalysis: ZnO-TiO_2 and TiO_2-ZnO core-shell structured heterojunction nanofibers via electrospinning and atomic layer deposition. Nanoscale, **6**, 5735, **2014**.
11. KADAM A., DHABBE R., GOPHANE A., SATHE T., GARADKAR K., Template free synthesis of ZnO/Ag_2O nanocomposites as a highly efficient visible active photocatalyst for detoxification of methyl orange. Journal of Photochemistry & Photobiology, B: Biology, **154**, 24, **2016**.
12. LIU G., LI G., QIU X., LI L. Synthesis of ZnO/titanate nanocomposites with highly photocatalytic activity under visible light irradiation. Journal of Alloys & Compounds, **481**, 492, **2009**.
13. QIU R., ZHANG D., MO Y., LIN S., BREWER E., HUANG X., XIONG Y., Photocatalytic activity of polymer-modified ZnO under visible light irradiation. Journal of Hazardous Materials, **156**, 80, **2008**.
14. SUN Y.Q., SUN Y., ZHANG T., CHEN G., ZHANG F., LIU D., CAI W., LI Y., YANG X., LI C. Complete Au@ZnO Core-Shell Nanoparticles with Enhanced Plasmonic Absorption Enabling Significantly Improved Photocatalysis. Nanoscale, **8**, 10774, **2016**.
15. Yu C.L., BAI Y., CHEN J.C., ZHOU W.Q., HE H.B., YU J.C., ZHU L.H., XUE S.S. Pt/Bi_2WO_6 composite microflowers: High visible light photocatalytic performance and easy recycle. Separation and Purification Technology, **154**, 115, **2015**.
16. KURIAKOSE S., CHOUDHARY V., SATPATI B., MOHAPATRA S. Facile synthesis of Ag-ZnO hybrid nanospindles for highly efficient photocatalytic degradation of methyl orange. Physical Chemistry Chemical Physics, **16**, 17560, **2014**.
17. YU C.L., YANG K., XIE Y., FAN Q.Z., YU J.C., SHU Q., WANG C.Y. Novel hollow Pt-ZnO nanocomposite microspheres with hierarchical structure and enhanced photocatalytic activity and stability. Nanoscale, **5**, 2142, **2013**.
18. DAS S., SINHA S., SUAR M., YUN S., MISHRA A., TRIPATHY S. K. Solar-photocatalytic disinfection of Vibria cholerae by using Ag@ZnO core-shell structure nanocomposites. Journal of Photochemistry Photobiology B: Biology, **142**, 68, **2015**.
19. PENG L., ZHE W., TONG W., QING P., YADONG L. Au-ZnO hybrid nanopyramids and their photocatalytic properties. The Journal of the American Chemical Society, **133**, 5660, **2011**.
20. LIU H.R., SHAO G.X., ZHAO J.F., ZHANG Z.X., ZHANG Y., LIANG J., LIU X.G., JIA H.S., XU B.S. Worm-Like Ag/ZnO Core-Shell Heterostructural Composites: Fabrication, Characterization, and Photocatalysis, The Journal of Physical Chemistry. C, **116**, 16182, **2012**.
21. LU F., CAI W., ZHANG Y. ZnO Hierarchical Micro/Nanoarchitectures: Solvothermal Synthesis and Structurally Enhanced Photocatalytic Performance &dagger. Advanced Functional Materials, **18**, 1047, **2008**.
22. YU C.L., ZHOU W.Q., LIU H., LIU Y., DINGYSUOU D.D. Design and fabrication of microsphere photocatalysts for environmental purification and energy conversion. Chemical Engineering Journal, **287**, 117, **2016**.
23. YU C.L., CAO F.F., LI X., LI G., XIE Y., YU J.C., SHU Q., FAN Q.Z., CHEN J.C. Hydrothermal synthesis and characterization of novel PbWO4 microspheres with hierarchical nanostructures and enhanced photocatalytic performance in dye degradation. Chemical Engineering Journal, **219**, 86, **2013**.
24. FANG W., YU C.L. Thermostability and photocatalytic performance of $BiOCl_{0.5}Br0.5$ composite microspheres. Journal of Materials Research, **30**, 3125, **2015**.
25. JING W.X., QI H., SHI J.F. JIANG Z.D., ZHOU F., CHENG Y.Y., GAO K. Effects of the geometries of microscale substrates on the surface morphologies of ZnO nanorod-based hierarchical structures. Applied Surface Science, **355**, 403, **2015**.
26. SARAVANAN R., KARTHIKEYAN N., GUPTA V.K., THIRUMAL E., THANGADURAI P., NARAYANAN V., STEPHEN A., ZnO/Ag nanocomposite: An efficient catalyst for degradation studies of textile effluents under visible light. Materials Science Engineering: C, **33**, 2235, **2013**.
27. LIN D., WU H., ZHANG R., PAN W. Enhanced Photocatalysis of Electrospun Ag-ZnO Heterostructured Nanofibers. Chemistry of Materials, **21**, 3479, **2009**.
28. ALAMMAR T., MUDRING A.V. Facile preparation of Ag/ZnO nanoparticles via photoreduction. Journal of Materials Science, **44**, 3218, **2009**.
29. ZHU G., LIU Y., XU H., CHEN Y., SHEN X., XU Z. Photochemical deposition of Ag nanocrystals on hierarchical ZnO microspheres and their enhanced gas-sensing properties. Crystengcomm, **14**, 719, **2011**.
30. MOSQUERA E., ROJAS-MICHEA C., MOREL M., GRACIA F., FUENZALIDA V., ZARATE R.A. Zinc oxide nanoparticles with incorporated silver: Structural, morphological, optical and vibrational properties. Applied Surface Science, **347**, 561, **2015**.
31. LIU T.Z., LI Y.Y., ZHANG H., WANG M., FEI X.Y., DUO S.W., CHEN Y., PAN J., WANG W. Tartaric acid assisted hydrothermal synthesis of different flower-like ZnO hierarchical architectures with tunable optical and oxygen vacancy-induced photocatalytic properties. Applied Surface Science, **357**, 516, **2015**.
32. TRIPATHY N., AHMAD R., KUK H., LEE D.H., HAHN Y.B., KHANG G. Rapid methyl orange degradation using

porous ZnO spheres photocatalyst. Journal of Photochemistry & Photobiology, B: Biology, **161**, 312, **2016**.
33. TANG D.M., LIU G., LI F., TAN J., LIU C., LU G.Q., CHENG H.M. Synthesis and Photoelectrochemical Property of Urchin-like Zn/ZnO Core-Shell Structures. The Journal of Physical Chemistry C, **113**, 11035, **2009**.
34. MOUDLER J.F., STICKLE W.F., SOBOL P.E., BOMBEN K.D. Handbook of X-ray Photoelectron Spectroscopy, Perkin-Elmer, Minnesota, **1992**.
35. DENG Q., TANG H.B., LIU G., SONG X.P., XU G.P., LI Q., NG D.H.L., WANG G.Z. The fabrication and photocatalytic performances of flower-like Ag nanoparticles/ZnO nanosheets-assembled microspheres. Applied Surface Science, **331**, 50, **2015**.
36. DENG Q., DUAN X., NG D.H.L., TANG H., YANG Y., KONG M., WU Z., CAI W., WANG G., Ag Nanoparticle Decorated Nanoporous ZnO Microrods and Their Enhanced Photocatalytic Activities, ACS Applied Materials & Interfaces. **4**, 6030, **2012**.
37. HUANG Q.L., ZHANG Q.T., YUAN S.S., ZHANG Y.C., ZHANG M. One-pot facile synthesis of branched Ag-ZnO heterojunction nanostructure as highly efficient photocatalytic catalyst. Applied Surface Science, **353**, 949, **2015**.
38. WU A.P., TIAN C.G., YAN H.J., HONG Y., JIANG B.J., FU H.G. Intermittent microwave heating-promoted rapid fabrication of sheet-like Ag assemblies and small-sized Ag particles and their use as co-catalyst of ZnO for enhanced photocatalysis. Journal of Materials Chemistry A, **2**, 3015, **2014**.
39. LIU H., HU Y., ZHANG Z., LIU X., JIA H., XU B. Synthesis of spherical Ag/ZnO heterostructural composites with excellent photocatalytic activity under visible light and UV irradiation, Appl. Surf. Sci., **355**, 644, **2015**.
40. LIANG Y., GUO N., LI L., LI R., JI G., GAN S. Fabrication of porous 3D flower-like Ag/ZnO heterostructure composites with enhanced photocatalytic performance. Applied Surface Science, **332**, 32, **2015**.
41. LAI Y., MING M., YU Y. One-step synthesis, characterizations and mechanistic study of nanosheets-constructed fluffy ZnO and Ag/ZnO spheres used for Rhodamine B photodegradation. Applied Catalysis B-Environmental., **100**, 491, **2010**.
42. LI J., WANG G., WANG H., TANG C., WANG Y., LIANG C., CAI W., ZHANG L. In situ self-assembly synthesis and photocatalytic performance of hierarchical $B_{i0.5}Na_{0.5}TiO_3$ micro/nanostructures. Journal of Materials Chemistry, **15**, 2253, **2009**.
43. FAGERIA P., GANGOPADHYAY S., PANDE S. Synthesis of ZnO/Au and ZnO/Ag nano-particles and their photocatalytic application using UV and visible light. Rsc Advances, **4**, 24962, **2014**.
44. WANG S., YU Y., ZUO Y., LI C., YANG J., LU C. Synthesis and photocatalysis of hierarchical heteroassemblies of ZnO branched nanorod arrays on Ag core nanowires. Nanoscale, **4**, 5895, **2012**.
45. BOUZID H., FAISAL M., HARRAZ F.A., AL-SAYARI S.A., ISMAIL A.A. Synthesis of mesoporous Ag/ZnO nanocrystals with enhanced photocatalytic activity, Catalysis Today, **252**, 20, **2015**.